Quarterly Report: Work Completed 12-31-2009

Methane Recovery from Hydrate-bearing Sediments

Funding Number: DE-FC26-06NT42963

Submitted By:

J. Carlos Santamarina
Georgia Institute of Technology
School of Civil and Environmental Engineering
Atlanta, GA 30332-0355
Phone: (404)-894.7605
Fax: (404)-894.2278
E-mail: jcs@gatech.edu

Costas Tsouris
Oak Ridge National Laboratory
Georgia Institute of Technology
School of Civil and Environmental Engineering
Atlanta, GA 30332-0373
E-mail: costas.tsouris@ce.gatech.edu

Acknowledgment: This material is based upon work supported by the Department of Energy under Award Number DE-FC26-06NT42963

INTRODUCTION - ANTICIPATED MAIN RESULTS

Goals: Identifying, understanding and modeling processes involved in methane production from hydrate-bearing sediments.

Approach: observation and interpretation of phenomena at multiple scales, ranging from pore-contact scale to the macro-reservoir scale, taking into consideration various possible driving forces (e.g., depressurization, thermal stimulation).

Anticipated results and most significant contributions: In view of our experience accumulated since the beginning of the project, we anticipate that some of the main results from this study will address:

- *Hydrate formation and growth*. Different conditions (unsaturated from gas phase, from ice, from dissolved phase, in water-wet and oil-wet sediments, during gas exchange). Formation rates at gas-water interface. Transients. Spatial distribution. *Relevance to marine and permafrost environments*.
- *Hydrate-mineral bonding and tensile strength*. Implications on the mechanical behavior oh hydrate bearing sediments in view of production strategies.
- *Gas production by heating and depressurization*. Study in 5m long 1D cell. Experimental study and modeling.
- *Gas production by chemo-driven methods*. Fundamental understanding of CO_2-CH_4 exchange
- *Gas production by transients*.
- *The role of effective stress* in formation and production.
- *Gas invasion versus gas production* – Evolution of degree of saturation and fluid conduction. Fluid-driven fractures.
- *Fluid conductivity in spatially varying sediments*
- *Thermodynamic formulation*
- *Coupled Thermo- Hydro- Chemo-Mechanical formulation*.
- *Production strategies in different formations*
- *Relevance to real systems*

Research Team: The current team is shown next.

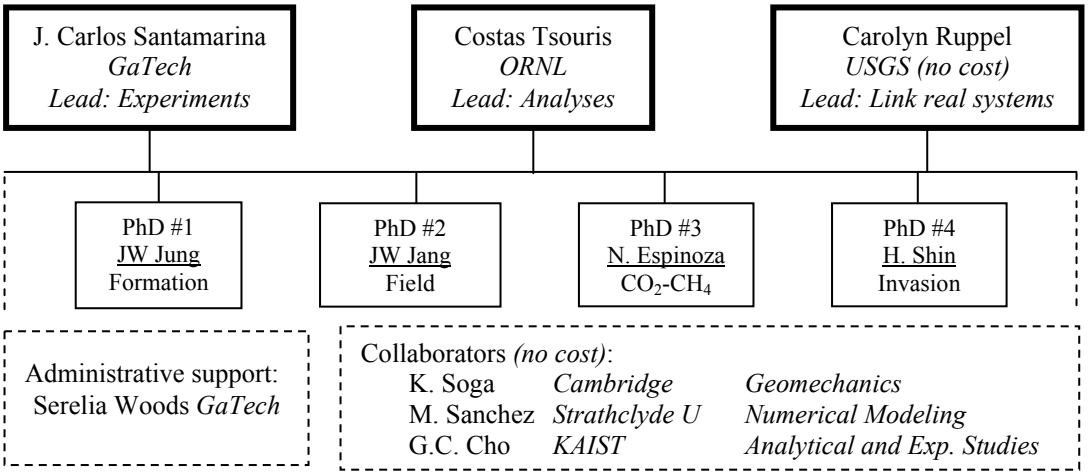

SUMMARY OF RESEARCH DEVELOPMENTS DURING THIS QUARTER

During this quarter, the research team has been dedicated to completing test sequences, advancing analyses, simulating numerical modeling and preparing manuscripts for all tasks reported in previous quarterly reports. The most relevant themes have included:

- CH_4-CO_2 replacement
    - Pore scale experimental study
    - Self-sustained CH_4-CO_2 hydrate replacement
    - Volume change during CH_4-CO_2 hydrate replacement
- Compilation of sediment characteristics of hydrate reservoirs
- Comparison of PT conditions at different reservoirs and implications on fluid expansion
- Gas recovery efficiency – Pore network modeling and macro-scale analyses

Salient results and observations are summarized next.

Experimental Device

Two different types of tests are conducted. The test configuration follows. Figure (a): Pressure cell and devices. Figure (a): Droplet experiments: i- CH_4 pressurization, ii- cooling, iii- CH_4 hydrate formation, iv- liquid CO_2 injection, v- CH_4-CO_2 hydrate dissociation. Figure (c): Meniscus experiments: i- CH_4 pressurization, ii- cooling, iii- ice formation, iv- ice melting, v- CH_4 hydrate formation, vi- injection of liquid CO_2, vii- liquid CO_2 to gas, viii- dissociation of CH_4 hydrate, and ix- dissociation of CO_2 hydrate. Both experiments are conducted using de-ionized water and research purity gases.

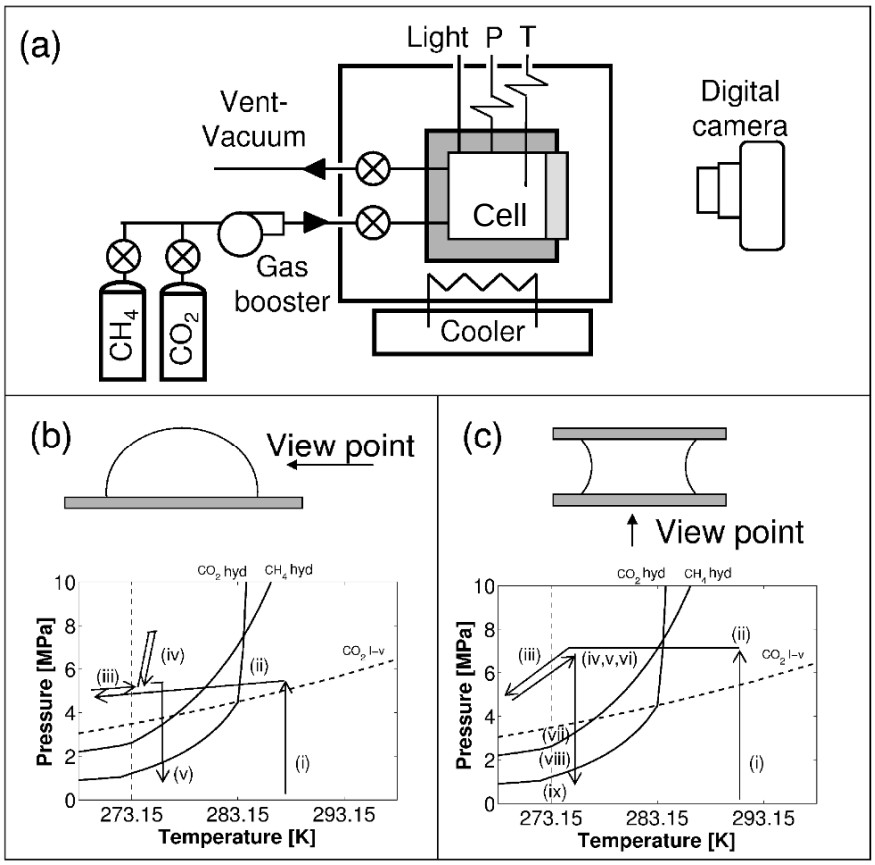

Droplet experiment

The following figures show the time evolution of the CH_4 hydrate shell after flooding with liquid CO_2. Pressure is 6MPa and the chamber temperature stays at 274±1K. This sequence of images shows that liquid CO_2 "dries" the water in droplet even in the presence of the hydrate shell.

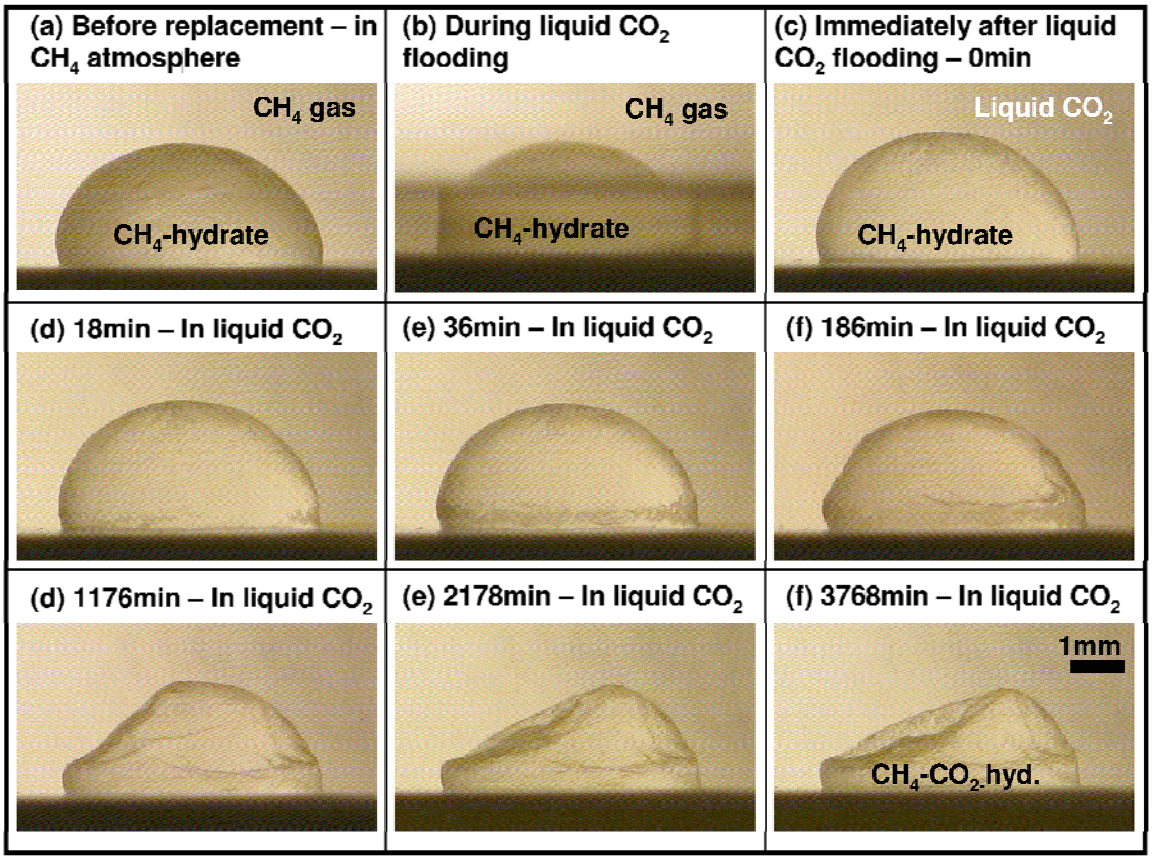

Meniscus experiment

(a) Water droplet – Scale: 8.7mm diameter, (b) Ice formation, (c) CH_4 hydrate formation and growth, (f) Injection of liquid CO_2, (g) Depressurization from liquid CO_2 to gas CO_2, (h) Image after crossing the CH_4 hydrate phase boundary

(a) 0min	(b) 140min	(c) 213min - In CH_4	(d) 901min – In CH_4
	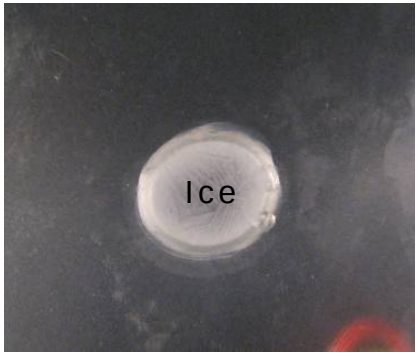		
(e) 1728min – In CH_4	(f) 1729min – In liquid CO_2	(g) 2086min – In gas CO_2	(h) 2090min – In gas CO_2
			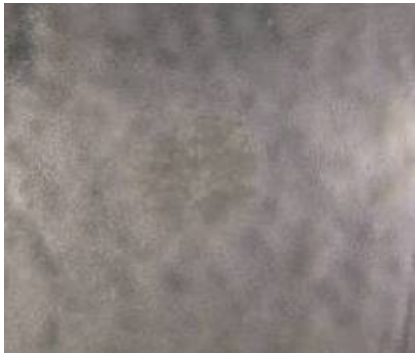

Self-sustained reaction within the CH_4 stability field

Pressure-temperature limits for self-sustained CH_4-CO_2 hydrate replacement based on heat released after CH_4 hydrate dissociation and CO_2 hydrate formation. Notice that a self-feeding reaction can occur far inside the CH_4 hydrate stability zone for a solid hydrate mass (~10K from the boundary). However, the self sustained reaction is only possible much closer to the CH_4 hydrate phase boundary in hydrate bearing sediments. Extra heat may be needed to promote hydrate replacement at high rate. Numerical results are obtained using the following equation and parameters c_m=0.83 kJ/(kg·K); H^f_{CDhyd}=395kJ/kg; and H^d_{Mhyd}=440kJ/kg.

$$T_o = T_b - \frac{\left(H^f_{CO2hyd}\rho_{CO2hyd} - H^d_{CH4hyd}\rho_{CH4hyd}\right) S_{hyd} n}{\rho_{CO2} S_{CO2} n\, c_{PCO2} + \rho_w S_w n\, c_{Pw} + \rho_{CH4hyd} S_{hyd} n\, c_{Phyd} + (1-n)\rho_m c_{Pm}}$$

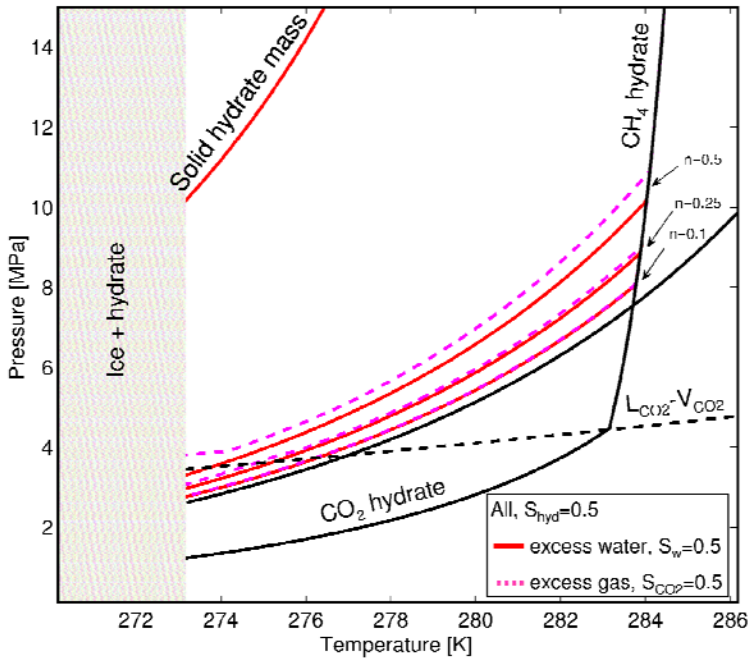

Volume change analysis at constant pressure

The figure shows:

(a) volume change during hydrate formation/dissociation. An initial volume of water expands V_{hyd}/V_w=1.234 to form CH_4 hydrate (n=6, ρ_{CH4hyd}=930kg/m^3), and V_{hyd}/V_w=1.279 to form CO_2 hydrate (n=6, ρ_{CO2hyd}=1110kg/m^3).

(b) volume change during CH_4-CO_2 replacement. Released CH_4 gas after replacement occupies a PT-dependent volume. The ratio is plotted in the figure show a very pronounced increase in pore fluid volume associated with CH_4-CO_2 replacement at constant pressure; for example, V_g^{CH4}/V_l^{CO2} = 480% at a constant 10MPa fluid pressure.

(a)

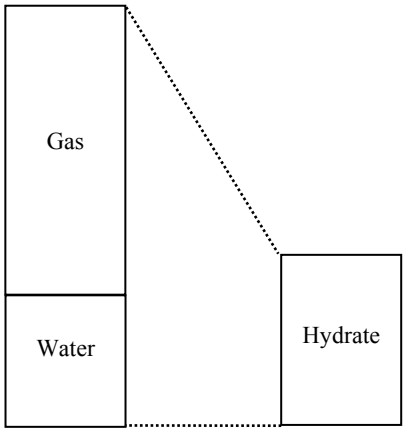

$$\frac{V_{CH_4\ hydrate}}{V_{water}} = 1.234$$

$$\frac{V_{CO_2\ hydrate}}{V_{water}} = 1.279$$

(b)

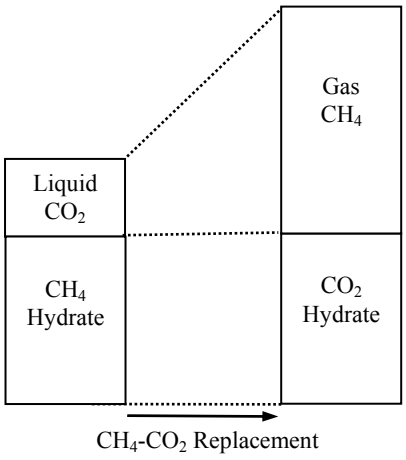

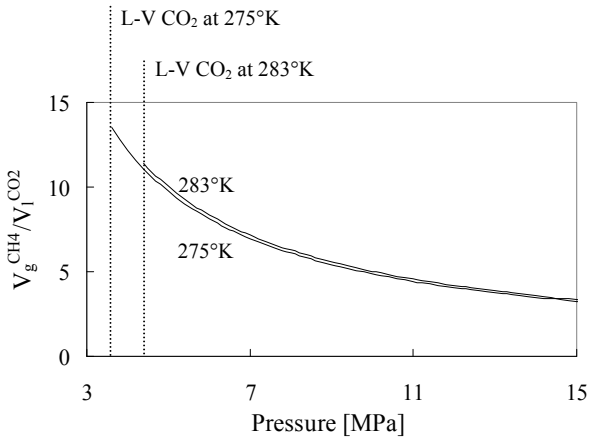

Hydrate reservoirs: PT conditions and fluid expansion during dissociation

Pressure and temperature condition for hydrate reservoirs worldwide are shown in the figure (to the left of the phase boundary). Lines of equal hydrate-to-fluid expansion ratio β are shown to the right. The fluid expansion factor β is equal to

$$\beta = \frac{V_g + V_w}{V_h} = \frac{nRT_g / P_g + V_w}{V_h} = \frac{\lambda V_h RT_g / (P_w + P_c) + 0.79V_h}{V_h} = \frac{\lambda RT_g}{P_w + 2T_s \cos\theta / R} + 0.79$$

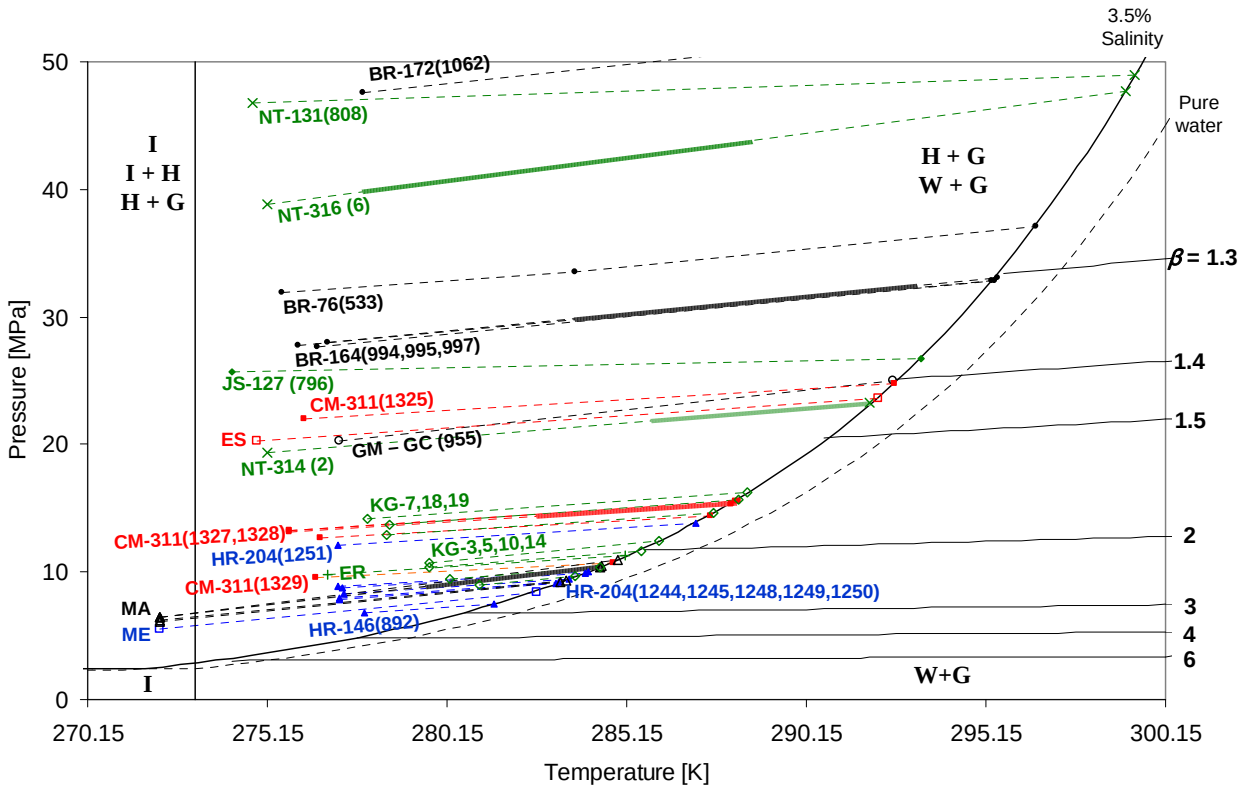

Plotted cases correspond to: (•) Blake Ridge BR [DSDP 76 (Site 533), ODP 164 (Site 994, 995, and 997), ODP 172 (Site 1062)], (×) Nankai Trough NT [ODP 131 (Site 808) IODP 314], (•) Japan Sea JS [ODP 127 (Site 796)], (■) Northern Cascadia Margin CM [ODP 146 (Site 889 and 890), IODP 311 (Site 1325, 1327, 1328, and 1329)], (□) East Sea (Korea) ES, (○) Gulf of Mexico GM [Green Canyon 955H], (◊) Krishna-Godavari (India) KG [NGHP 01 (3,5,7,10,14,18, and 19)], (▲) Hydrate Ridge HR [ODP 146 (Site 892), ODP 204 (Site 1244, 1245, 1248, 1249, 1250, and 1251)], (+) Eel River Basin (California) ER [ODP 167 (Site 1019)], (Δ) Mallik MA [2~5L-38] and (□) Mt. Elbert ME ME-01. Phase transformation boundaries for pure water [Kwon et al., 2008] and for 3.5% salinity water [*Sloan*] are shown. We assume no solubility of methane gas in water and constant mass density for water.

Pore-network model

A new concept of pore-network model is developed for this study. A pore-network model consists of pores interconnected by throats. (a) Hydrate starts to dissociate and release gas when β>1. (b) Gas occupies the initially hydrate-filled pore when β≈1.8. (c) Gas expands into neighboring pores as expansion increases beyond β>1.8.

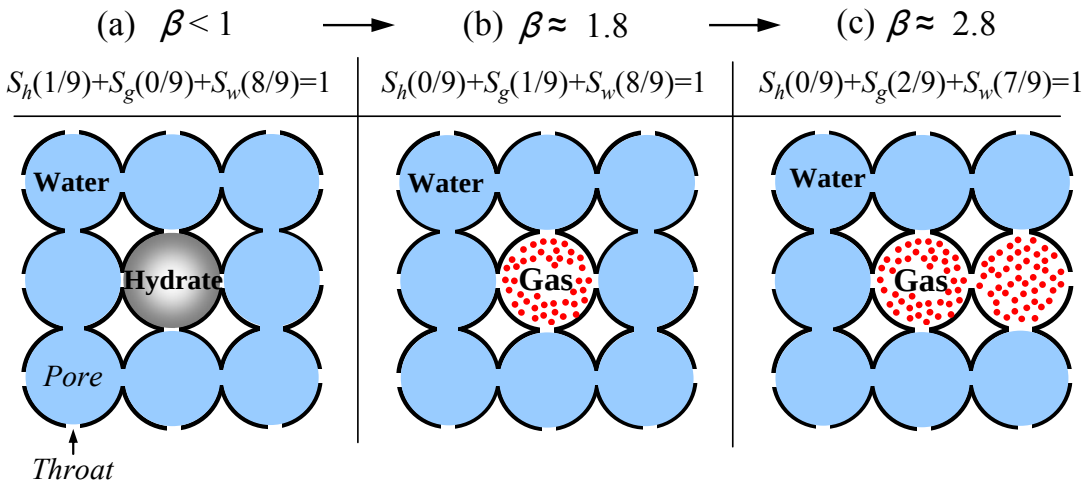

Initial hydrate distribution and evolution of gas saturation

Initial hydrate distribution and the expansion of gas clusters are shown in the figure. A single drainage boundary is placed on left side. Figure (a): Initial hydrate distribution for a hydrate saturation of S_h=10%; uncorrelated random distribution is assumed. Figure (b)~(d): Gas cluster formation during gas expansion; the different colors indicate: gas pores connected to the drainage boundary (light blue), isolated gas pores (yellow), and water pores (dark blue). Two-dimensional pore network model: 50×50 pores, randomly distributed pore radius with constant mean $\mu(R_p)$=1μm and standard deviation $\sigma[\ln(R_p)]$=0.4. The throat radius R_{th} between two neighboring pores is equal to half of the minimum of the two pore radii $R_{th}=0.5\cdot min(R_p^1, R_p^2)$.

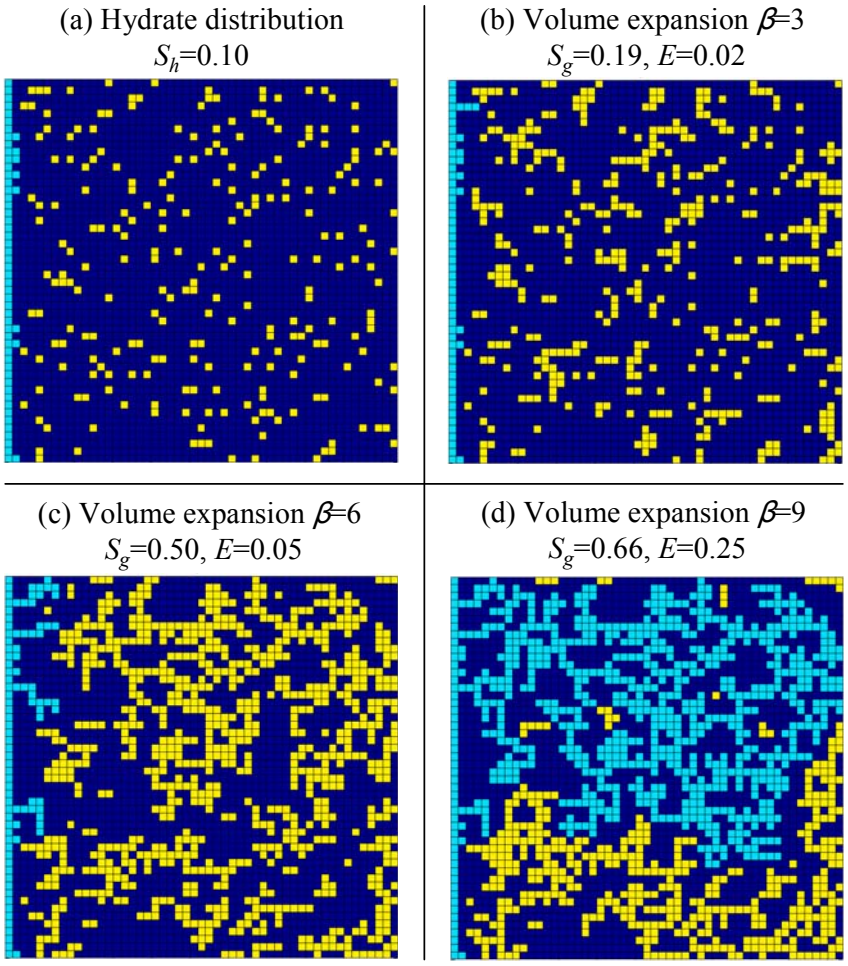

Gas recovery efficiency and residual saturation

The initial hydrate saturation was varied from S_h=5 to S_h=40% while keeping the mean pore size $\mu(R_p)$=1μm and the standard deviation of pore size $\sigma[\ln(R_p)]$=0.4 constant. The gas recovery efficiency E increases as the expansion factor increases at a given initial hydrate saturation, and at given gas expansion, high initial hydrate saturation results in high gas recovery efficiency.

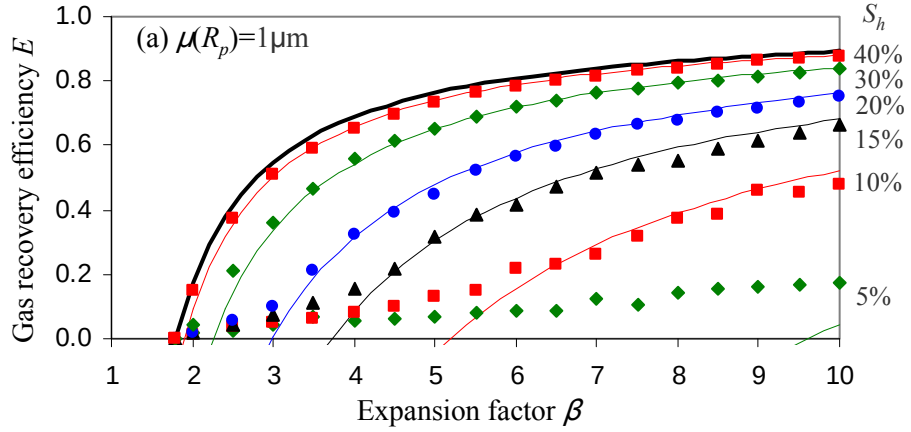

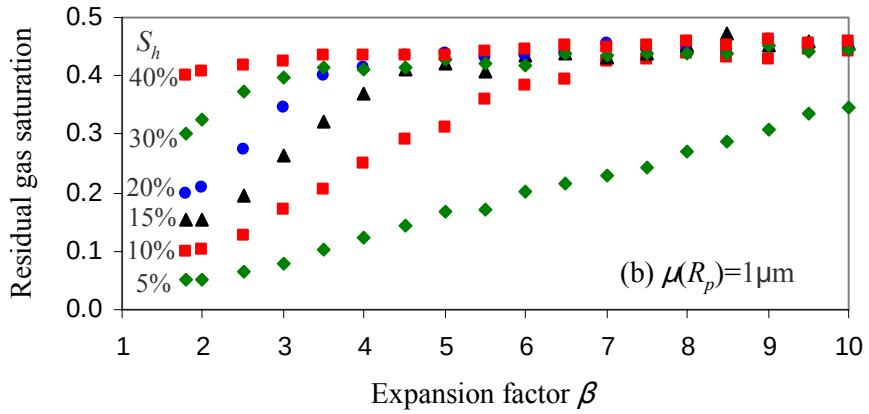

Macro-scale analysis for gas recovery efficiency

Gas recovery efficiency can be estimated using macro-scale analyses. The figure shows the initial hydrate and water saturations, followed by the produced gas and water for several cases. The ratio of the water volume V_w^{dis} from dissociation to the initial hydrate volume V_h^{ini} is $V_w^{dis}/V_h^{ini}\approx 0.79$, and the volume of the gas and water from dissociation $V_g^{dis}+V_w^{dis}$ is equal to βV_h^{ini}. In all cases, the gas recovery efficiency depends on the gas expansion factor, residual gas saturation, and initial hydrate saturation.

General case. Gas displaces some water and occupies some pores.

$$E=\frac{V_g^{rec}}{V_g^{dis}}=\frac{V_g^{dis}-V_g^{res}}{V_g^{dis}}=\frac{\beta V_h^{ini}-0.79V_h^{ini}-V_g^{res}}{\beta V_h^{ini}-0.79V_h^{ini}}$$

$$=\frac{\beta-0.79-S_g^{res}/S_{hyd}}{\beta-0.79}\quad (0.21S_h\le S_g^{res}\le 1)$$

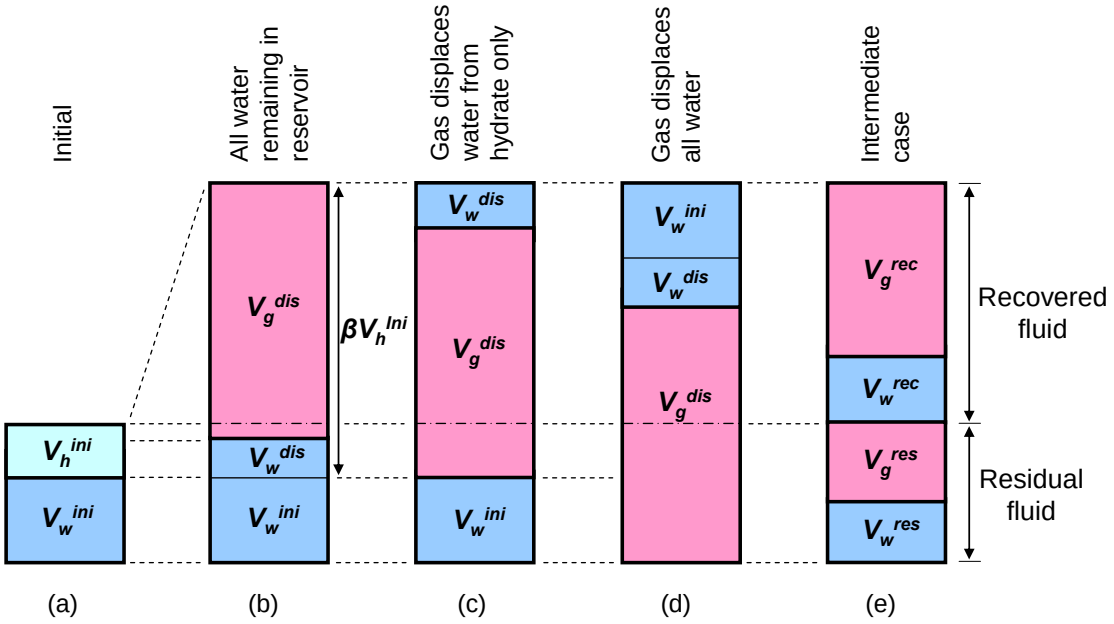

(a) Initial hydrate and water. (b) $S_g^{res}=0.21S_h$. (c) $S_g^{res}=S_h$. (d) $S_g^{res}=1$. (e) General case.